

pubs.acs.org/crystal Article

Steric Perturbation to a Channel Hydrate: The Limits of Isomorphism

Taylor A. Watts, Courtney E. Lee, Sara M. Niederberger, Jeffery A. Bertke, and Jennifer A. Swift*



Cite This: Cryst. Growth Des. 2021, 21, 5889-5896



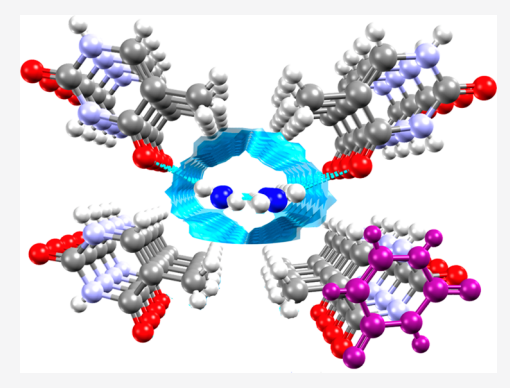
ACCESS I

III Metrics & More



Supporting Information

ABSTRACT: Thymine hydrate (**TH**) is a classic hydrate system in which water molecules are highly confined in linear one-dimensional channels. Here, we describe our efforts to tune the channel volume by preparing isomorphous mixed crystals with increasing concentrations of uracil (Ur) and 5-ethyluracil (EUr), molecular analogues with slightly smaller and larger volumes, respectively. Solutions with up to 20 mol % Ur successfully yielded isomorphous mixed crystals of TH-Ur_x in phase-pure form, though analysis of the mixed crystal compositions indicated that only ~46% of the Ur available in the initial growth solution was proportionately included in the host lattice. The thermal stability of the mixed TH-Ur_x material was significantly altered, with a greater fraction of water loss occurring at low temperature compared to the pure hydrate phase. Isomorphous mixed crystals with EUr substitutions, TH-EUr_x , were successfully prepared from solutions with 5–10 mol % EUr, although the fraction of EUr



included was much lower (\sim 13–36%) than Ur. As the concentration of EUr in the growth solution increased to 15–20 mol %, an unexpected mixed composition anhydrate emerged as the dominant crystallization product. Although packing fraction estimates suggested that higher EUr substitution levels in the hydrate were theoretically possible, the formation of the mixed anhydrate presented a more favorable route to a dense material phase.

■ INTRODUCTION

An important prerequisite in the design of robust organic crystalline materials is a thorough understanding of structure—property relationships. Organic molecular hydrates are a ubiquitous class of crystalline materials^{1,2} encountered in the production of fine chemicals (e.g., active pharmaceutical ingredients³), yet their thermal stabilities remain difficult to predict.^{4–8} Often sensitive to environmental conditions (e.g., temperature and relative humidity), many molecular hydrates are susceptible to partial or complete water loss. Since the physical properties of a crystalline compound depend on its structure (e.g., solubility, mechanical strength), there is considerable interest in defining the structural factors^{9–16} that dictate water loss from hydrated phases and the potential products that result from solid state dehydration reactions.

The DNA nucleobase thymine (aka 5-methyluracil) crystallizes as a classic channel hydrate ^{17,18} from aqueous solution. Several solid state computational and experimental investigations have focused on this hydrate system since its structure was first reported in 1961. ^{9,15,19–25} Gerdil referred to the structure as a monohydrate with 80% water occupancy in the original crystal structure report. ¹⁹ More recent calculations by Braun et al. ¹⁵ indicated that the channels are too small to enable a monohydrate composition, and the authors referred to it as a 0.8-hydrate to better reflect its stoichiometry. We refer to it here by the simpler term thymine hydrate (TH). Like most channel hydrates, TH has a limited thermal stability range and is prone to dehydration via a diffusive mechanism. ²⁵

Although the **TH** lattice can tolerate some partial degree of water loss, water loss above a critical threshold results in the collapse of the hydrate lattice and the conversion to anhydrous crystalline forms.

In previous work, ²⁶ we demonstrated it was possible to systematically replace a fraction of the thymine molecules in TH with 5-aminouracil substitutions. Since the 5-methyl groups of thymine define the boundaries of the water channels in TH, we reasoned that mixed crystals would place 5-amino groups at the surface of the water channels but not otherwise disrupt the layered packing motif. Though few previous solid solution studies have reported amino/methyl substitutions, the similarity in the volume of the two substituents made mixed crystal formation remarkably effective. Mixed crystals with up to ~18 mol % 5-aminouracil content (~85% of that available in solution) were isomorphous with TH, and the addition of the hydrogen bonding amino groups at the water channel surface imparted the hydrate with significantly greater thermal stability than the pure material.

Here we explore mixed crystal formation with other uracil components (Scheme 1), which upon inclusion in the TH

Received: July 1, 2021

Published: September 7, 2021





Scheme 1. Molecular Structures of Thymine, Uracil (Ur), and 5-Ethyluracil (EUr)

$$\begin{array}{c|c} & & & \\ &$$

lattice locally increase or reduce the volume of the water channel. Direct 1-for-1 replacement of a fraction of thymine molecules with uracil was expected to increase the channel volume owing to the smaller size of a hydrogen atom (2.0 ų)²⁷ relative to a methyl group (\sim 23 ų).^{27,28} Direct 1-for-1 replacement of thymine molecules with 5-ethyluracil (EUr) would place larger 5-ethyl (\sim 40 ų)^{27,28} substituents in the 5-methyl sites, with any excess substituent volume potentially extending into the water channels as needed. Through this mixed hydrate approach, we hoped to better understand (a) the tolerance limits of the TH lattice for substituents with more diverse steric requirements and (b) how subtle steric modifications made to the water channels affect the overall thermal stability of the hydrate.

■ EXPERIMENTAL SECTION

Sample Preparation. Anhydrous thymine (Sigma-Aldrich, ≥99%), uracil (Ur, Sigma, >99%) and 5-ethyluracil (EUr, Alfa Aesar, >98%) were used without further purification. Ultrapure 18.2 $M\Omega$ water from an Elga Purelab Flex system was used in all crystal preparations. Thymine hydrate (TH) crystals were prepared from 5 mg/mL aqueous thymine solutions maintained at 4 °C. Optically transparent (010) plates typically formed in the supersaturated solutions within 12 h. Mixed crystals of TH-Ur, and TH-EUr, were prepared similarly, starting with 5 mg/mL aqueous solutions of handground mixtures of thymine and either Ur or EUr in fixed stoichiometric ratios where the mole fraction of Ur was progressively increased. In our mixed crystal nomenclature, the x in TH-Ur, and TH-EUr, corresponds to the mole fraction of Ur or EUr in the growth solution; e.g., TH-Ur₅, TH-Ur₁₀, TH-Ur₁₅, and TH-Ur₂₀ were obtained from solutions with 5, 10, 15, and 20 mol % Ur, respectively. Mixed crystals typically appeared in the 4 °C aqueous solutions within

Sample Characterization. Optical micrographs were obtained on an Olympus BX-50 polarizing microscope fitted with a Lumenera Xfinity 2.0 camera and Xfinity Analyze software (Lumenera, Ontario). Room temperature powder X-ray diffraction (PXRD) data from $2\theta = 5-50^\circ$ were collected on either a DUO Apex X-ray diffractometer or a Rigaku Ultima instrument (Cu Kα radiation, 50 kV, 30 mA current). PXRD data on the DUO were obtained on lightly ground samples in Kapton capillaries (Cole-Parmer, 0.0320″ ID × 0.0340″ OD, 12″ L). Data were integrated using APEX-2 software and analyzed using Panalytical X'Pert Highscore Plus software.

For each mixed composition that yielded phase-pure **TH-Ur**_x and **TH-EUr**_x material by PXRD, the average 5-X-uracil and water content were determined through ¹H NMR and thermogravimetric analysis (TGA), respectively.

 1 H NMR (DMSO- d_{6}) data on triplicate dissolved TH-Ur_x and TH-EUr_x samples were collected on a 400 MHz Varian Inova Spectrometer. Triplicate TGA data on TH-Ur_x and TH-EUr_x were obtained on a TA Instruments SDT Q600 instrument (New Castle, DE). Samples were heated at 5.0 °C/min from 25 to 120 °C under a nitrogen flow rate of 50 mL/min. All experiments used 3.0–5.0 mg of as-grown material in 90 μL alumina cups (TA Instruments).

Thermal transitions in each mixed $TH-Ur_x$ and $TH-EUr_x$ phase were evaluated with differential scanning calorimetry (DSC) using either a TA Instruments model Q200 or model Q50. As-grown

samples (3–5 mg) were heated in hermetically sealed aluminum pans at 5.0 °C/min over the temperature range 25–120 °C. The dehydration temperature reported for each sample, $T_{\rm max}$ is the peak temperature of the integrated thermograms and an average of at least triplicate measurements.

Single Crystal Structure Determination. X-ray diffraction data on single crystals of TH, TH-Ur₅, TH-Ur₁₀, TH-EUr₅, TH-EUr₁₀, and T-EUr₂₀ were collected on either a Bruker D8 Quest diffractometer equipped with a Mo ImS source and a Photon 100 CMOS detector or a Bruker DUO equipped with a Mo fine-focus sealed source and an APEXII CCD detector (Bruker-AXS). A series of 0.5° φ - and ω -scans were collected with monochromatic Mo K α radiation ($\lambda = 0.71073$ Å) at 100 K and integrated with the Bruker SAINT program. Structure solution and refinement was performed using the SHELXTL/PC suite and ShelXle. All single crystal structures were solved by intrinsic methods and refined using fullmatrix least-squares on F^2 using SHELXT-Version 2014/5 and SHELXL-2018/3 software.³⁰ All non-hydrogen atoms were modeled anisotropically while hydrogen atoms were treated with a mixture of independent and constrained refinement parameters often using riding idealized contributor models. Additional refinement details for individual structures are provided in the Supporting Information.

The single crystal structure of TH-Ur₁₅ was determined at 100 K by single crystal synchrotron X-ray diffraction at ChemMatCARS Sector 15 at the Advanced Photon Source. Frames were collected using ϕ -scans in a Bruker platform 3-circle goniometer with fixed chi equipped with a Dectris PILATUS 100 detector, λ = 0.41328 Å, an undulator beam, and a diamond [111] crystal, and two mirrors (to exclude higher harmonics) in the beam path. Data collection and unit cell refinement were carried out with SMART. CCDC deposition: 2085477–2085479, 2085481–2085483

■ RESULTS AND DISCUSSION

The crystal structure of **TH** is shown in Figure 1. In this channel hydrate, thymine molecules assemble into one-dimensional hydrogen bonded tapes which close-pack into extended π -stacks to create dense layers in the (010) plane. The interface between the thymine layers has a comparatively lower molecular density, where linear channels created along the \pm *c*-axis are occupied with water molecules. As previously stated, the water occupancy is ~80%. Each water channel is bounded on two sides by the 5-methyl groups of thymine molecules and has a cross-sectional diameter of ~3.2 Å at the narrowest point. The highly confined water molecules within a given channel hydrogen bond to one another $(O_w \cdots O_w = 2.55$ Å) as well as to the O4 atoms of neighboring thymine molecules $(O_w \cdots O_4 = 2.84 \text{ Å})$.

In order to assess how steric perturbations at the water channel surface affect the structure and properties of TH, we set out to prepare two series of mixed crystal isomorphs wherein a secondary component, either uracil (Ur) or 5ethyluracil (EUr), would replace a fraction of thymine molecules in the lattice. Ur substitutions were seen as a way to subtly increase the available volume of the channels. EUr substitutions were envisioned as a means to subtly reduce the channel volume. While the substitution of heteromolecules with similar to slightly smaller sizes than the host is generally thought to be less disruptive to the lattice, ^{27,31-35} EUr inclusion was thought to be viable since they would not interrupt the hydrogen bonding and π stacking within the dense layers and the increased substituent size could potentially be offset by changes in the water occupancy within the channels. Neither Ur or EUr are known to crystallize independently in a hydrated form.²² Assuming there was some practical limit in the mole fraction of the secondary component that could be included in the TH lattice, we examined

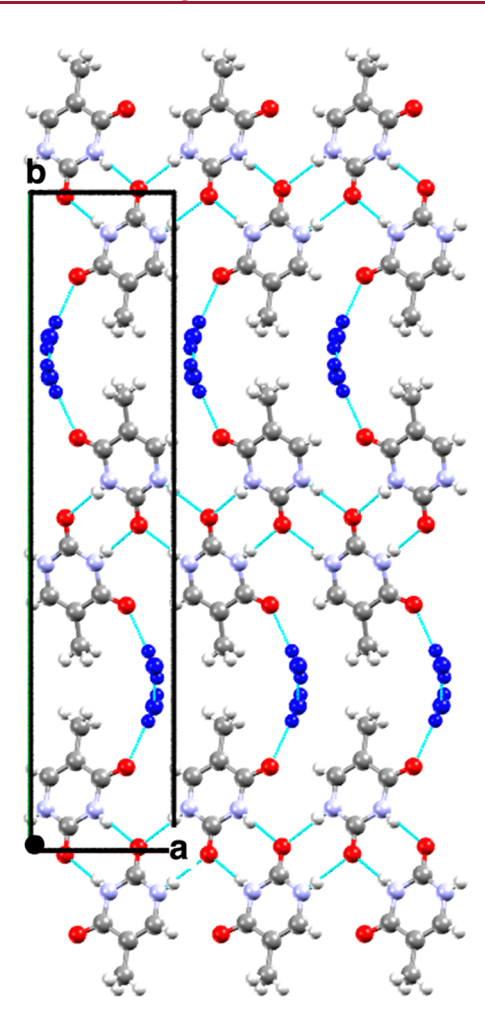
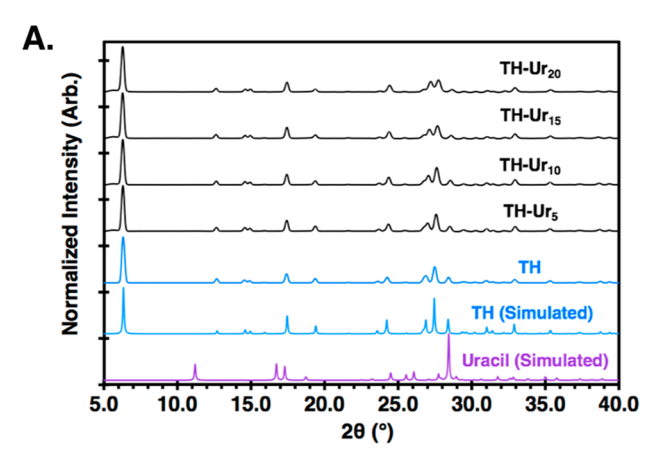


Figure 1. Molecular structure of thymine hydrate viewed down the one-dimensional water channel (*c*-axis).

conditions that would support Ur or EUr inclusion of up to a maximum of 20 mol %. Efforts to create mixed thymine hydrate lattices with 5–20 mol % Ur or EUr are discussed in separate sections below.

Mixed Crystals of Thymine and Uracil (TH-Ur). Supersaturated aqueous solutions (5 mg/mL) of thymine and 5–20 mol % uracil (Ur) were prepared in four different stoichiometric ratios. Higher ratios were not attempted. When maintained at 4 °C, all solutions crystallized within ~12 h. We refer to the mixed crystals as TH-Ur₅, TH-Ur₁₀, TH-Ur₁₅, and TH-Ur₂₀, where the subscript corresponds to the mole fraction of uracil in the growth solution. Powder X-ray diffraction (PXRD) patterns of the bulk material from each mixed solution composition had an identical pattern to that of TH (Figure 2A). The absence of any additional diffraction lines in the PXRD, including those associated with anhydrous uracil, ³⁶ indicated the bulk material was phase-pure.

The average Ur concentration in material obtained from each solution composition was determined by solution ^{1}H NMR based on the ratio of the integrated intensities of the C6-H signal from thymine (δ = 7.24, singlet) and Ur (δ = 7.38, doublet) of dissolved crystals. Over the 5–20 mol % Ur solution range examined, there was an approximately linear relationship between the Ur concentration in the growth solution and in the resulting solid. On average, this equated to an inclusion of ~46% of the available Ur in solution. **TH-Ur**₅,



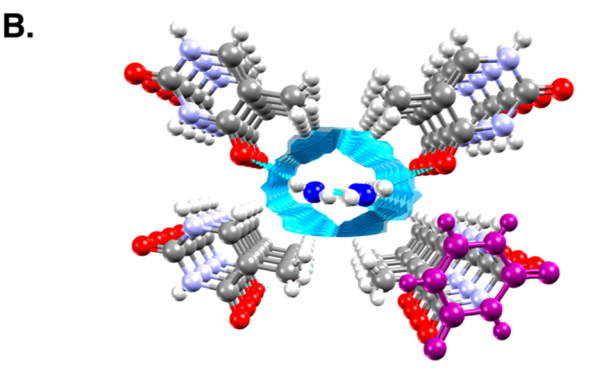


Figure 2. (A) Comparison of PXRD patterns of **TH-Ur**_x crystals grown from aqueous solutions with 5–20 mol % Ur against the actual and simulated PXRD patterns of **TH.** (B) Molecular representation of Ur (purple) inclusion in **TH-Ur** viewed down the water channel. The water space was calculated using the Mercury Hydrate Analyzer tool using a probe radius of 1.0 Å.

TH-Ur₁₀, TH-Ur₁₅, and TH-Ur₂₀ mixed crystals had average Ur concentrations of 2.5(5), 5.0(1.2), 6.15(8), and 8.8(5) mol %, respectively.

Whereas pure TH crystallizes from aqueous solution as plates with large (010) faces and typical dimensions of $0.5 \times 0.15 \times 0.1$ mm, the addition of Ur to the growth solution led to an overall reduction in the crystal size and a relative reduction in the growth rate along the \pm *b*-axis (Figure S1) such that the plates were exceptionally thin. Since the 5-methyl groups project from the (010) surfaces, it is reasonable that inclusion of Ur primarily affects the growth of these faces. The very thin plate morphologies are consistent with what one expects based on tailor-made additive effects. TH-Ur₁₀, and TH-Ur₁₅, although TH-Ur₁₅ required a synchrotron source due to the small size of the crystalline materials obtained (Table 1).

In developing a structure model for each $TH-Ur_x$ composition, the thymine:Ur ratio was fixed based on the component ratios determined by solution 1H NMR while the water molecule occupancies were allowed to freely refine. When organic component occupancies were allowed to freely refine based on electron density, the ratios were typically within 0.5–1% of those determined by solution NMR. This suggests while there may be slight compositional differences from crystal to crystal within a batch, the magnitude of those variations is likely small. In each case, the uracil molecules were assumed to include in the same orientation as the thymine molecules which they replace (Figure 2B) since this enables

Table 1. Crystallographic Parameters for All Single Crystal Structures Determined in This Work^a

system	TH	TH-Ur ₅	TH-Ur ₁₀	TH-Ur ₁₅ ^b
formula	$C_5H_6N_2O_2\cdot 0.84(H_2O)$	0.98 C ₅ H ₆ N ₂ O ₂ , 0.02 C ₄ I 0.81(H ₂ O)	$H_4N_2O_2$ · 0.95 $C_5H_6N_2O_2$, 0.05 C_4H_4N 0.83 (H_2O)	C_2O_2 · 0.94 $C_5H_6N_2O_2$, 0.06 $C_4H_4N_2O_2$ · 0.80(H_2O)
temperature (K)	100	100	100	100
space group	$P2_1/c$	$P2_1/c$	$P2_1/c$	$P2_1/c$
a (Å)	5.9979(5)	6.0065(12)	5.9899(6)	5.984(8)
b (Å)	27.724(2)	27.750(5)	27.792(3)	27.82(4)
c (Å)	3.7452(3)	3.7408(8)	3.7271(4)	3.724(5)
β (deg)	93.170(3)	93.107(6)	92.947(4)	93.227(12)
vol (ų)	621.82(9)	622.6(2)	619.63(11)	619.0(15)
Z	4	4	4	4
R-factor (%)	4.22	6.41	7.15	12.45
crystal habit	plate	plate	thin plate	thin plate
system	TH	-EUr ₅	TH-EUr ₁₀	$ ext{T-EUr}_{20}$
formula	0.982 C ₅ H ₆ N ₂ O ₂ , 0.01	8 C ₆ H ₈ N ₂ O ₂ ·0.82 (H ₂ O)	$0.987 \ C_5H_6N_2O_2$, $0.013 \ C_6H_8N_2O_2$. 0.81	(H_2O) 0.77 $(C_5H_6N_2O_2)$, 0.23 $(C_6H_8N_2O)$
temperature (K)	100		100	100
space group	$P2_1/c$		$P2_1/c$	C2/m
a (Å)	5.9975(7)		6.0029(4)	6.543(7)
b (Å)	27.771(3)		27.7732(17)	6.822(2)
c (Å)	3.7413(5)		3.7353(2)	26.3385(12)
β (deg)	93.192(4)		93.187(2)	94.090(17)
vol (ų)	622.18(13)		621.79(7)	1172.5(13)
Z	4		4	8
R-factor (%)	5.18		4.62	8.46
crystal habit	plate		plate	plate

 $[^]a$ Wherever possible, the occupancies of thymine and Ur or EUr components were fixed based on integrated 1 H NMR intensities. Water occupancies were freely refined. b Synchrotron XRD structure.

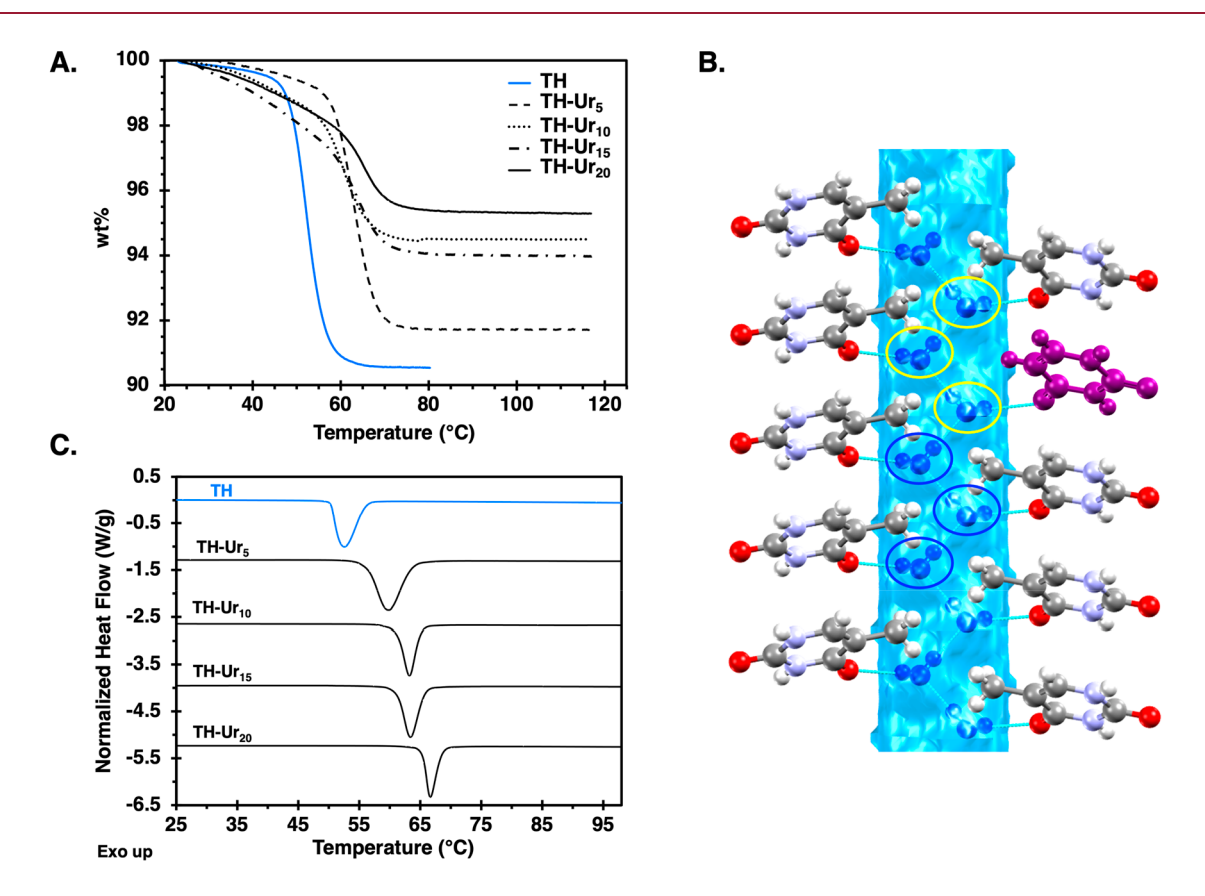


Figure 3. (A) Thermogravimetric analysis of TH-Ur_x compositions compared against TH. (B) Schematic of a TH-Ur_x water channel. The included Ur molecule is shown in purple; the local environment around some water molecules is significantly altered by Ur inclusion (yellow circles) while other water sites more distant to the Ur inlusion are less affected by the Ur (blue circles). (C) Differential scanning calorimetry thermograms of TH and TH-Ur_x.

the hydrogen bonding motif to be conserved. The diffraction data do not strictly rule out the possibility of whole molecule disorder where the C2=O and C4=O positions of the included Ur are reversed. However, a Ur molecule in this alternative orientation would weaken the hydrogen bonded tape. If whole molecule disorder were present in \mathbf{TH} - \mathbf{Ur}_x it would be extremely difficult to identify given the low % of Ur in the lattice and the similarity in the electron densities of N1 and C5.

Refinement of the water occupancy in each of the TH-Ur, single crystal diffraction data sets yielded water content comparable to pure TH. However, thermogravimetric analysis (TGA) of the samples revealed a more complicated picture of both the water content and the water loss. The TGA weight loss curve of TH is sigmoidal, but as the Ur content in TH-Ur, increases, the shape of the TGA curve changes and an increasing fraction of water loss occurs at lower temperatures before the final major water loss event (Figures 3A, S3). We suspect that some water loss may also occur during sample preparation, despite efforts to collect thermograms as quickly as possible after the TH-Ur_x samples are removed from the growth solution. The water content reflected in the TGA curves of TH-Urx is likely lower than the actual value. Assuming all compositions of TH-Ur_x have the same initial water stoichiometry, increasing the Ur content makes it easier for the majority of water loss to occur at lower temperatures compared to pure TH.

The random distribution of Ur substitutions in the crystal creates a variety of different local sites which water molecules can occupy. The model in Figure 3B provides an idealized cross-sectional view of a one-dimensional water channel where one Ur molecule (purple) replaces a thymine molecule. The water molecules at the substitution site (circled in yellow) experience a different local steric environment compared to water molecules occupying sites more distant from the inclusion site (circled in blue). While cooperativity effects presumably also play a role here, the water mobilities in yellow and blue sites likely differ. Water loss at Ur substitution sites appears more facile, since an increase in the number of these substitution sites results in a smaller fraction of water loss at the final highest temperature. We note that the DSC thermograms (Figure 3C, Table S1) show that the T_{max} actually increases with Ur inclusion $(T_{\text{max}} (\text{TH}) = 54.4(7)^{\circ}$ vs T_{max} (TH-Ur₂₀) = 66.2(9)°), suggesting that the final transformation to anhydrous material may be sensitive to other factors. On the molecular level, solid state dehydration is determined by a multitude of inter-related factors (e.g., diffusion rates along regular vs heterogeneous channels, cooperativity among water molecules) which are difficult to assess and to decouple from the other events (e.g., mechanical collapse to an anhydrous lattice).

Thymine and 5-Ethyluracil Mixtures. Supersaturated aqueous solutions (5 mg/mL) of thymine and 5, 10, 15, and 20 mol % 5-ethyluracil (EUr) were prepared and allowed to crystallize at 4 °C. PXRD analysis of the bulk material resulting from each mixed composition showed that only the 5 mol % EUr solution had a pattern consistent with phase-pure **TH-EUr**₅ (**Figure 4**). The 10 and 15 mol % EUr solutions showed diffraction lines corresponding to **TH-EUr**_x as well as some other phase. The 20 mol % EUr solution yielded exclusively this second phase, which proved to be an anhydrous mixed crystal of thymine and EUr, **T-EUr**_x.

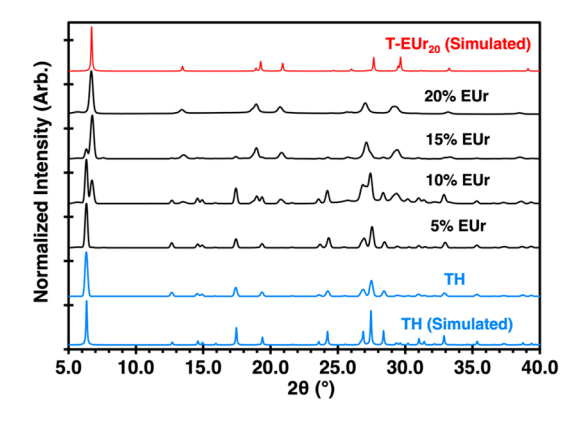
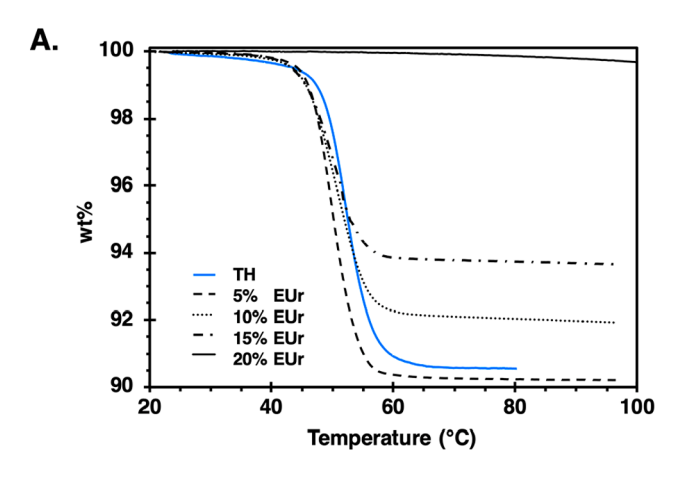


Figure 4. Comparison of PXRD patterns of bulk material grown from aqueous solutions with 5-20 mol % EUr. Data are compared against the simulated PXRD patterns of **TH** and the simulated structure of an anhydrous mixed crystal grown from 20 mol % EUr solution, **T-EUr**₂₀.

X-ray diffraction of single crystals isolated from TH-EUr₅ and TH-EUr₁₀ batches proved to be isomorphous with TH (Table 1). ¹H NMR analysis of the dissolved TH-EUr₅ sample indicated 1.8(2) mol % of included EUr, or ~36% of that available in the growth solution. This NMR ratio was used in the development of the TH-EUr₅ structure model. Because the bulk sample from the 10% EUr solution was a phase mixture, the % EUr included in TH-EUr₁₀ was determined based on the electron densities in the diffraction data rather than ¹H NMR. The optimized model yielded 1.3 mol % EUr, which would mean inclusion of $\sim 13\%$ of the EUr initially present in the growth solution. In both the TH-EUr, and TH-EUr₁₀ structures, the 5-ethyluracil was found to replace a thymine molecule in the expected 1-for-1 orientation. Although the ethyl groups are conformationally flexible, there was no evidence in the diffraction data that they are rotationally disordered at 100 K.

Refinement of the TH- EUr_5 and TH- EUr_{10} water occupancies indicated in both cases a 0.8 stoichiometry similar to pure TH. For TH- EUr_5 , this is consistent with the weight loss observed from TGA (Figure 5A). The TGA weight loss observed from bulk material obtained from 10% and 15% EUr solutions was less, owing to the fact that the samples contain increasing amounts of the second anhydrous phase. Notably, the TH- EUr_x generated from the 5, 10, and 15% EUr solutions all exhibited the same sigmoidal dehydration profile as TH. The 20% EUr solutions yielded only anhydrous material, so TGA showed no water loss.

The structure of the mixed anhydrous phase was determined from X-ray diffraction of single crystals isolated from bulk T-EUr₂₀ (Figure 6). ¹H NMR analysis of dissolved bulk T-EUr₂₀ indicated an average EUr content of 23.0(1.1)%. T-EUr₂₀ has an asymmetric unit consisting of two independent molecules and a C2/m unit cell with dimensions a = 6.543(7) Å, b = 6.822(2) Å, c = 26.3385(12) Å, $\beta = 94.090(17)^{\circ}$, and Vol = 1172.5(13) Å³. Each molecular site was modeled with substitutional disorder fixed to match the ¹H NMR ratios. Whole molecule rotational disorder was also evident at each site, with the O4 and C6-H positions (and N1-H and N3-H) exchanged. Each diffraction line in the bulk material obtained from the 20 mol % EUr solution is accounted for by the simulated PXRD pattern. Similarly, all of the diffraction lines in the bulk material obtained from the 10 and 15 mol % EUr



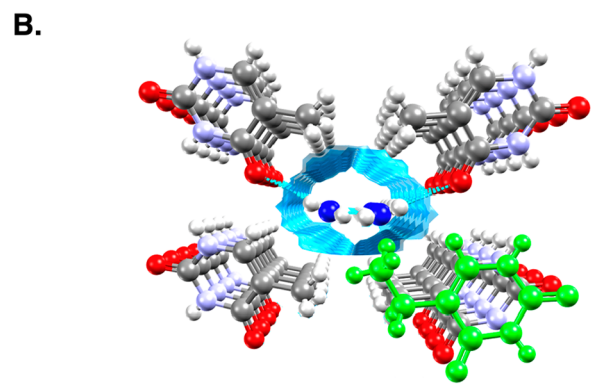


Figure 5. (A) Thermogravimetric analysis of bulk material obtained from growth solutions containing 5, 10, 15, and 20 mol % EUr. (B) Molecular representation of EUr (green) inclusion in **TH-EUr**_x (x = 5, 10, 15) viewed down the water channel. The water-accessible space was calculated using the Mercury Hydrate Analyzer tool using a probe radius of 1.0 Å.

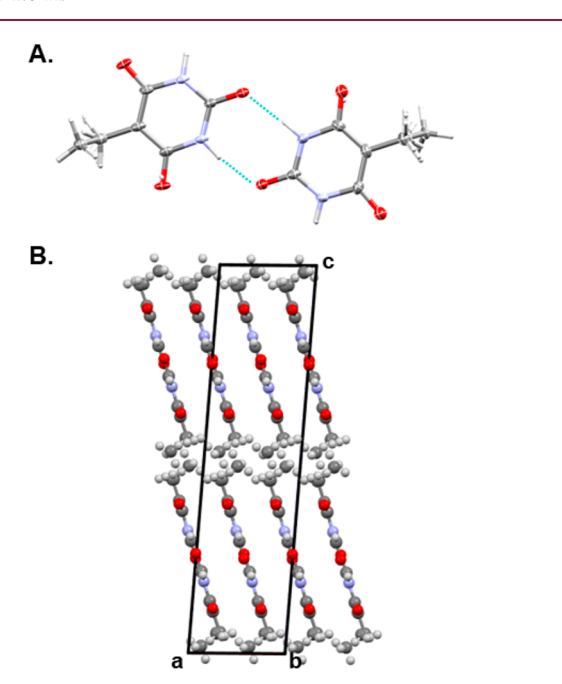


Figure 6. (A) Asymmetric unit in T-EU r_{20} . Thermal ellipsoids are represented at 50% probability. (B) Expanded view of the crystal packing in T-EU r_{20} viewed down the hydrogen bonded tapes which form along the b-axis.

solutions that do not correspond to $TH-EUr_x$ match to peaks in the simulated PXRD of $T-EUr_{20}$.

In most molecular crystal systems, this agreement in PXRD patterns would support an interpretation that the 20% EUr solution yielded phase-pure material from and a binary mixture of hydrate and anhydrate from the 10% and 15% solutions. However, given the demonstrated propensity for uracil derivatives to exhibit polytypism, 22 and the remarkable similarity in the PXRD patterns of some 5-X-uracil polymorphs with polar and nonpolar hydrogen bonded tape motifs, 39 solutions which yield T-EUr, may also yield anhydrous polytypes and/or crystals with differing degrees of molecular order/disorder. Addressing this open question would be challenging owing to the small crystal sizes obtained under these growth conditions. Notably, T-EUr₂₀ is not an isomorph of the experimental 5-ethyluracil structure (refcode: BOLLIY) which has a well-ordered nonpolar tape motif and a different arrangement of ethyl groups at the interface between the dense molecular layers (Figure S8).

Packing Density Considerations. In an attempt to rationalize the change from $TH-EUr_x$ to $T-EUr_x$ as the EUr concentration in the growth solution increased, we compared the packing coefficient and solvent-accessible void space in the two forms (Table 2). The pure TH structure at 100 K has an

Table 2. Packing Coefficient and Solvent-Accessible Void Space Calculated Using Mercury and the PLATON Squeeze $Tool^a$

theoretical composition	packing coefficient	solvent-accessible volume (\mathring{A}^3) per unit cell
TH (full water occupancy)	0.742	187
TH (no water)	0.640	
TH-EUr ₅ with 100% EUr (full water occupancy)	0.778	154
TH-EUr ₅ with 100% EUr (no water)	0.699	
T-EUr ₂₀ (with 100% thymine)	0.730	
T-EUr ₂₀ (with 100% EUr)	0.808	
TH-Ur ₅ with 100% Ur (full water occupancy)	0.650	258
TH-Ur ₅ with 100% Ur (no water)	0.546	

^aA probe radius = 0.3 Å was used for PLATON calculations.

estimated packing fraction of \sim 0.72, based on calculated packing fractions of models where the water occupancy is fixed at 100% or 0%. This is within the typical 0.65–0.77 range for molecular crystals cited by Kitaigorodsky.²⁷

Using the mixed crystal $\mathbf{TH}\text{-}\mathbf{EUr}_5$ structure and ShelXle, 30 a hypothetical model was created with an 5-ethyluracil in every organic site by deleting the thymine molecule from the original model. As one would expect, this artificial structure with 100% EUr would have a higher estimated packing fraction ~ 0.76 assuming a water occupancy of 80%. Although this still falls within the typical packing fraction range, EUr substitution proved to be not a particularly effective strategy for increasing the molecular density because only a small fraction of the available EUr in the growth solution was found to include in the \mathbf{TH} lattice. No doubt this is related to the fact that the mixed anhydrate phase $\mathbf{T}\text{-}\mathbf{EUr}_{20}$ served as an unexpected alternative. It is more complicated to accurately estimate the packing fraction of this phase given the molecular disorder. However, hypothetical structures (without disorder) with

100% thymine or 100% EUr in the lattice have estimated packing fractions of 0.73 and 0.81, respectively. A structure with 23% EUr content would have an estimated packing fraction of \sim 0.75, which is also more dense than the pure TH lattice. As the EUr concentration in the growth solution increases, formation of the mixed anhydrate presumably offers a superior way to achieve higher density.

A similar packing fraction analysis was performed on TH-Ur_x where Ur substitution was expected to lead to materials less dense than pure TH. Using the mixed TH-Ur₅ structure and shelXle, a hypothetical model was created with a uracil in every organic site. This artificial structure with 100% uracil would have a packing fraction \sim 0.65, which would be on the low end of Kitaigorodsky's range.

The solvent-accessible void space in the 100% 5-ethyluracil, 100% thymine, and 100% uracil hydrate lattices was also calculated using Mercury software 41 and the PLATON Squeeze tool 42,43 (0.3 Šsqueeze probe). Once the water was removed, as expected, the 100% uracil lattice showed the highest solvent-accessible volume per unit cell (~258 ų), followed by the 100% thymine lattice (~190 ų) and the 100% 5-ethyl lattice (~154 ų). Yet despite the large theoretical changes in the water-accessible void space that could be achieved in the TH-EUr_x and TH-Ur_x mixed crystals, the diffraction data suggested the water content does not substantially change across the various mixed crystal compositions.

CONCLUSIONS

Overall, the different inclusion behaviors of uracil and 5ethyluracil in TH lattices suggest that steric considerations can have a large effect on the ability to create mixed crystal hydrates. Although both Ur and EUr have molecular structures that allow for preservation of the dominant hydrogen bonding and π stacking interactions in the dense TH layers, the size of the functional group at the 5-X position creates a sensitive perturbation. The higher inclusion tolerance for Ur than EUr in the TH lattice is consistent with the notion that it is easier to replace a host molecule with a structural mimic that has a slightly smaller (vs slightly larger) volume, a premise that has been discussed in other literature. 27,31,32,34,35 Nevertheless, the unexpected appearance of T-EUr₂₀ highlights the general difficulty in predicting crystallization outcomes in mixed systems. It is not obvious how one could rationally anticipate what (if any) alternative mixed crystal forms, such as T-EUr₂₀₁ may result when secondary components with similar core structures but slightly different peripheral groups are added to the growth solution.

ASSOCIATED CONTENT

Supporting Information

The Supporting Information is available free of charge at https://pubs.acs.org/doi/10.1021/acs.cgd.1c00761.

Optical micrographs, NMR, TGA, and DSC data (PDF)

Accession Codes

CCDC 2085477–2085479 and 2085481–2085483 contain the supplementary crystallographic data for this paper. These data can be obtained free of charge via www.ccdc.cam.ac.uk/data_request/cif, or by emailing data_request@ccdc.cam.ac.uk, or by contacting The Cambridge Crystallographic Data Centre, 12 Union Road, Cambridge CB2 1EZ, UK; fax: +44 1223 336033.

AUTHOR INFORMATION

Corresponding Author

Jennifer A. Swift — Department of Chemistry, Georgetown University, Washington, DC 20057-1227, United States; orcid.org/0000-0002-8011-781X; Email: jas2@georgetown.edu

Authors

Taylor A. Watts — Department of Chemistry, Georgetown University, Washington, DC 20057-1227, United States Courtney E. Lee — Department of Chemistry, Georgetown University, Washington, DC 20057-1227, United States

Sara M. Niederberger – Department of Chemistry, Georgetown University, Washington, DC 20057-1227, United States

Jeffery A. Bertke — Department of Chemistry, Georgetown University, Washington, DC 20057-1227, United States; orcid.org/0000-0002-3419-5163

Complete contact information is available at: https://pubs.acs.org/10.1021/acs.cgd.1c00761

Notes

The authors declare no competing financial interest.

ACKNOWLEDGMENTS

The authors gratefully acknowledge financial support from the Henry Luce Foundation (TAW Clare Boothe Luce Predoctoral Fellowship) and the National Science Foundation (DMR 1609541 and 2004435). We thank Yu-Sheng Chen for his assistance with collecting synchrotron PXRD data. NSF's ChemMatCARS Sector 15 is supported by the Divisions of Chemistry (CHE) and Materials Research (DMR), National Science Foundation, under grant number NSF/CHE-1834750. Use of the Advanced Photon Source, an Office of Science User Facility operated for the U.S. Department of Energy (DOE) Office of Science by Argonne National Laboratory, was supported by the U.S. DOE under Contract No. DE-AC02-06CH11357.

REFERENCES

- (1) Infantes, L.; Fábián, L.; Motherwell, W. D. S. Organic crystal hydrates: what are the important factors for formation. *CrystEngComm* **2007**, *9*, 65.
- (2) Gillon, A. L.; Feeder, N.; Davey, R. J.; Storey, R. Hydration in Molecular Crystals A Cambridge Structural Database Analysis. *Cryst. Growth Des.* **2003**, 3 (5), 663–673.
- (3) Khankari, R. K.; Grant, D. J. W. Pharmaceutical hydrates. *Thermochim. Acta* **1995**, 248, 61–79.
- (4) Griesser, U. J. The Importance of Solvates. In *Polymorphism*; Hilfiker, R., Ed.; Wiley, 2006; pp 211–233.
- (5) Stahly, G. P. Diversity in Single- and Multiple-Component Crystals. The Search for and Prevalence of Polymorphs and Cocrystals. *Cryst. Growth Des.* **2007**, *7* (6), 1007–1026.
- (6) van de Streek, J.; Motherwell, S. New software for searching the Cambridge Structural Database for solvated and unsolvated crystal structures applied to hydrates. *CrystEngComm* **2007**, *9*, 55–64.
- (7) Görbitz, C. H.; Hersleth, H.-P. On the inclusion of solvent molecules in the crystal structures of organic compounds. *Acta Crystallogr., Sect. B: Struct. Sci.* **2000**, *BS6*, 526–534.
- (8) Werner, J. E.; Swift, J. A. Data mining the Cambridge Structural Database for hydrate—anhydrate pairs with SMILES strings. *CrystEngComm* **2020**, 22, 7290–7297.
- (9) Perrier, P. R.; Byrn, S. R. Influence of Crystal Packing on the Solid-State Desolvation of Purine and Pyrimidine Hydrates: Loss of Water of Crystallization from Thymine Monohydrate, Cytosine

- Monohydrate, 5-Nitrouracil Monohydrate, and 2'-Deoxyadenosine Monohydrate. *J. Org. Chem.* **1982**, 47, 4671–4676.
- (10) Brittain, H. G.; Morris, K. R.; Boerrigter, S. X. M. Structural Aspects of Solvatomorphic Systems. In *Polymorphism in Pharmaceutical Solids*, 2nd ed.; Brittain, H. G., Ed.; CRC Press, 2009; pp 233–281.
- (11) Zhou, D.; Schmitt, E. A.; Zhang, G. G. Z.; Law, D.; Wight, C. A.; Vyazovkin, S.; Grant, D. J. W. Model-free treatment of the dehydration kinetics of nedocromil sodium trihydrate. *J. Pharm. Sci.* **2003**, *92*, 1367–1376.
- (12) Braun, D. E.; Koztecki, L. H.; Mcmahon, J. A.; Price, S. L.; Reutzel-Edens, S. M. Navigating the Waters of Unconventional Crystalline Hydrates. *Mol. Pharmaceutics* **2015**, *12*, 3069–3088.
- (13) Lee, J.; Kim, D.; Park, J.; Kim, E. E.; Lah, M. S.; Kim, A. Pseudopolymorphs of LB30870, a Direct Thrombin Inhibitor: One-Dimensional Solvent Channel Structures Explain Reversible Hydration/Dehydration. *Cryst. Growth Des.* **2018**, *18*, 95–104.
- (14) Braun, D. E.; Griesser, U. J. Stoichiometric and Non-stoichiometric Hydrates of Brucine. *Cryst. Growth Des.* **2016**, *16*, 6111–6121.
- (15) Braun, D. E.; Gelbrich, T.; Wurst, K.; Griesser, U. J. Computational and Experimental Characterization of Five Crystal Forms of Thymine: Packing Polymorphism, Polytypism/Disorder, and Stoichiometric 0.8-Hydrate. *Cryst. Growth Des.* **2016**, *16*, 3480–3496.
- (16) Kiang, Y.-H.; Cheung, E.; Stephens, P. W.; Nagapudi, K. Structural Studies of a Non-Stoichiometric Channel Hydrate Using High Resolution X-ray Powder Diffraction, Solid-State Nuclear Magnetic Resonance, and Moisture Sorption Methods. *J. Pharm. Sci.* **2014**, *103*, 2809–2818.
- (17) Morris, K. R. Structural Aspects of Hydrates and Solvates. In *Polymorphism in Pharmaceutical Solids*; Brittain, H. G., Ed.; Marcel Dekker, Inc.: New York, 1999; pp 125–181.
- (18) Morris, K. R.; Rodriguez-Hornado, N. Hydrates. In *Encyclopedia of Pharmaceutical Technology*, Vol. 7; Swarbrick, J., Boylan, J. C., Eds.; Dekker: New York, 1993; pp 393–440.
- (19) Gerdil, R. The crystal structure of thymine monohydrate. *Acta Crystallogr.* **1961**, *14*, 333–344.
- (20) Ozeki, K.; Sakabe, N.; Tanaka, J. The crystal structure of thymine. Acta Crystallogr., Sect. B: Struct. Crystallogr. Cryst. Chem. 1969, 25, 1038–1045.
- (21) Portalone, G.; Bencivenni, L.; Colapietro, M.; Pieretti, A.; Ramondo, F.; Møller, J.; Senning, A.; Yao, X.-K.; Wang, H.-G.; Tuchagues, J.-P.; Ögren, M. The Effect of Hydrogen Bonding on the Structures of Uracil and Some Methyl Derivatives Studied by Experiment and Theory. *Acta Chem. Scand.* **1999**, *53*, 57–68.
- (22) Barnett, S. A.; Hulme, A. T.; Issa, N.; Lewis, T. C.; Price, L. S.; Tocher, D. A.; Price, S. L. The observed and energetically feasible crystal structures of 5-substituted uracils. *New J. Chem.* **2008**, 32, 1761.
- (23) Chennuru, R.; Muthudoss, P.; Ramakrishnan, S.; Mohammad, A. B.; Ravi Chandra Babu, R.; Mahapatra, S.; Nayak, S. K. Preliminary studies on unusual polymorphs of thymine: Structural comparison with other nucleobases. *J. Mol. Struct.* **2016**, *1120*, 86–99.
- (24) Ahlqvist, M. U. A.; Taylor, L. S. Water dynamics in channel hydrates investigated using H/D exchange. *Int. J. Pharm.* **2002**, 241, 253–261.
- (25) Watts, T. A.; Miehls, E. K.; Swift, J. A. Time-Resolved Cooperative Motions in the Solid-State Dehydration of Thymine Hydrate. *Cryst. Growth Des.* **2020**, *20*, 7941–7950.
- (26) Watts, T. A.; Niederberger, S. M.; Swift, J. A. Improving Channel Hydrate Stability via Localized Chemical Tuning of the Water Environment. *Cryst. Growth Des.* **2021**, *21*, 5206.
- (27) Kitaigorodsky, A. I. Structure of Crystals. In *Molecular Crystals and Molecules*, Vol. 29; Academic Press Inc., 1973; pp 1–133.
- (28) Bondi, A. van der Waals Volumes and Radii. J. Phys. Chem. 1964, 68 (3), 441-451.
- (29) Degen, T.; Sadki, M.; Bron, E.; König, U.; Nénert, G. The HighScore suite. *Powder Diffr.* **2014**, *29*, S13–S18.

- (30) Hubschle, C. B.; Sheldrick, G. M.; Dittrich, B. ShelXle: a Qt graphical user interface for SHELXL. *J. Appl. Crystallogr.* **2011**, *44*, 1281–1284.
- (31) Kitaigorodskii, A. I. Mixed Crystals, Vol. 33; Springer-Verlag: Berlin, 1984.
- (32) York, P.; Grant, D. J. W. A disruption index for quantifying the solid state disorder induced by additives or impurities. I. Definition and evaluation from heat of fusion. *Int. J. Pharm.* **1985**, 25 (1), 57–72.
- (33) Lusi, M. Engineering Crystal Properties through Solid Solutions. Cryst. Growth Des. 2018, 18 (6), 3704–3712.
- (34) Lusi, M. A rough guide to molecular solid solutions: design, synthesis and characterization of mixed crystals. *CrystEngComm* **2018**, 20 (44), 7042–7052.
- (35) Schur, E.; Nauha, E.; Lusi, M.; Bernstein, J. Kitaigorodsky Revisited: Polymorphism and Mixed Crystals of Acridine/Phenazine. *Chem. Eur. J.* **2015**, 21 (4), 1735–1742.
- (36) Stewart, R. F.; Jensen, L. H. Redetermination of the crystal structure of uracil. *Acta Crystallogr.* **1967**, 23 (6), 1102–1105.
- (37) Berkovitch-Yellin, Z.; Van Mil, J.; Addadi, L.; Idelson, M.; Lahav, M.; Leiserowitz, L. Crystal morphology engineering by "tailormade" inhibitors; a new probe to fine intermolecular interactions. *J. Am. Chem. Soc.* **1985**, *107* (11), 3111–3122.
- (38) Weissbuch, I.; Addadi, L.; Lahav, M.; Leiserowitz, L. Molecular Recognition at Crystal Interfaces. *Science* **1991**, *253*, 637–645.
- (39) Copley, R. C. B.; Barnett, S. A.; Karamertzanis, P. G.; Harris, K. D. M.; Kariuki, B. M.; Xu, M.; Nickels, E. A.; Lancaster, R. W.; Price, S. L. Predictable Disorder versus Polymorphism in the Rationalization of Structural Diversity: A Multidisciplinary Study of Eniluracil. *Cryst. Growth Des.* **2008**, 8 (9), 3474–3481.
- (40) Watts, T. A.; Price, L. S.; Price, S. L.; Niederberger, S. M.; Bertke, J. A.; Swift, J. A. The Crystal Structure of 5-Aminouracil and the Ambiguity of Alternative Polymorphs. *Isr. J. Sci.*, **2021**, DOI: 10.1002/ijch.202100062.
- (41) Macrae, C. F.; Sovago, I.; Cottrell, S. J.; Galek, P. T. A.; McCabe, P.; Pidcock, E.; Platings, M.; Shields, G. P.; Stevens, J. S.; Towler, M.; Wood, P. A. Mercury 4.0: from visualization to analysis, design and prediction. *J. Appl. Crystallogr.* **2020**, *53* (1), 226–235.
- (42) Spek, A. Single-crystal structure validation with the program PLATON. *J. Appl. Crystallogr.* **2003**, *36* (1), 7–13.
- (43) Spek, A. L. PLATON SQUEEZE: a tool for the calculation of the disordered solvent contribution to the calculated structure factors. *Acta Crystallogr., Sect. C: Struct. Chem.* **2015**, *71*, 9–18.